Localization of Ca^{++}-containing Antimonate Precipitates during Mitosis

SUSAN M. WICK and PETER K. HEPLER

Botany Department, University of Massachusetts, Amherst, Massachusetts 01003; The Marine Biological Laboratory, Woods Hole, Massachusetts 02543; and Department of Biological Sciences, Stanford University, Stanford, California 94305. Dr. Wick's present address is the Department of Developmental Biology, Research School of Biological Sciences, The Australian National University, Canberra, A. C. T. 2601, Australia.

ABSTRACT   Intracellular bound Ca^{++} has been localized throughout mitosis and cytokinesis in two plant species by means of *in situ* precipitation with potassium antimonate and electron microscope visualization. Identification of Ca^{++} as the major cation precipitated was made by comparing solubility properties in water, EDTA, and EGTA of the intracellular deposits with respect to those of K^{+}-, Mg^{++}-, and Ca^{++}-antimonate standards. In spermatogenous cells of the water fern, *Marsilea vestita*, and stomatal complex cells of barley, *Hordeum vulgare*, antimonate deposits have been found associated with the endoplasmic reticulum (ER), vacuoles, euchromatin/nucleoplasm, and mitochondria. The last contain a much higher density of precipitates in *Marsilea* than in *Hordeum*. Dictyosomes and the nuclear envelope of *Marsilea* also contain antimonate deposits, as do the plasmalemma, cell wall, and phragmoplast vesicles of *Hordeum*. Microtubule-organizing centers such as kinetochores and the blepharoplast of *Marsilea* do not stain. In spite of differences in associated antimonate between certain organelles of the two species, the presence of antimonate along the ER throughout the cell cycle is common to both.

Of particular interest are those precipitates seen along the tubules and cisternae of the extensive smooth ER that surrounds and invades the mitotic spindle in both species. The ability to bind divalent cations makes the mitotic apparatus (MA)-associated ER a likely candidate for regulation of free Ca^{++} levels in the immediate vicinity of structural components and processes that are Ca^{++}-sensitive and proposed to be Ca^{++}-regulated.

There have been numerous reports on in vitro binding and uptake of Ca^{++} by mitochondria and various microsomal fractions. In addition, studies concerning in vivo Ca^{++}-buffering capabilities (4, 20, 24, 35, 36) and the ultrastructural localization of Ca^{++} *in situ* in several cell and tissue types have recently appeared (summarized in footnote 1). The story emerging from this work seems to be that all cells possess organelles that can function as sarcoplasmic reticulum (SR) equivalents by alternately sequestering and releasing Ca^{++}, thereby regulating free Ca^{++} levels in the cell and the myriad cellular processes known or proposed to be under the influence of Ca^{++} (3, 12, 13, 16, 17, 27). The accumulating evidence includes little information on sequestration sites in plant cells, however, or on the distribution of these sites throughout the processes of mitosis and cytokinesis.

The localization of Ca^{++} sequestration sites during mitosis and cytokinesis becomes particularly significant in light of various observations on the involvement of Ca^{++} in these processes. The structural integrity of mitotic apparatus (MA) microtubules in vivo (20, 21) and in isolated MAs (33, 38, 39), and the rates of mitosis and cytokinesis (1, 45) have been shown to be sensitive to Ca^{++}. Moreover, release from meiotic arrest of some invertebrate (8, 28) and mammalian (10, 44) oocytes is triggered by Ca^{++}.

Because Ca^{++} affects the structure and function of the MA as well as the triggering of mitosis, the ability to control intracellular Ca^{++} levels in the nucleus and in the vicinity of

---

[1] Wick, S. M., and P. K. Hepler. Selective localization of intracellular bound Ca^{++} with potassium antimonate. Manuscript in preparation.

the subsequently formed spindle must be important to the cell. A suggestion that the MA indeed contains Ca^{++}-regulating elements comes from the description of a membrane-bound, Ca^{++}-activated ATPase in the MA of various cells (25, 30). Ca^{++} uptake has also been shown to be associated with the MA in vivo (20, 21) and in vitro (41, 42). It seems likely that the ER which is associated with the MA, surrounding it (11, 17, 40), often producing membrane "caps" in polar regions of plant cells (31), and lying alongside spindle fibers or near chromosomes, is responsible for this sequestration (see references 12, 14, and 16 for reviews).

This study was undertaken to examine, by means of antimonate precipitation, the distribution of bound or sequestered Ca^{++} through mitosis and cytokinesis and, in particular, to determine whether the MA-associated membranes are capable of binding Ca^{++} and are thereby possibly involved in the regulation of Ca^{++} levels within the spindle. We demonstrate that, under the conditions employed here, antimonate selectively precipitates cellular Ca^{++} and can thus be used as a probe for Ca^{++}-binding and sequestration sites. We find that elements of ER, shown previously to have a close structural association with the mitotic apparatus of plant cells (16, 17), are prime compartments for the accumulation of Ca^{++} within dividing cells. This evidence implicates the MA-associated endoplasmic reticulum (ER) in the regulation of Ca^{++} levels during mitosis.

MATERIALS AND METHODS

Tissue Sources

Sporocarps of the water fern *Marsilea vestita* were ground briefly in a Braun electric coffee grinder. Microspores were separated from megaspores and sporocarp wall debris by means of a series of graded stainless-steel sieves (Newark Wire Cloth Co., Newark, N. J.) and were stored in tightly capped vials at room temperature until used. Microspores were grown either in 50 mM potassium phosphate buffer, pH 6.8, or in Laetsch's fern culture solution (22), minus Ti $(SO_4)_3$, at 20°C and at a density of 8-15 mg/10 ml of solution. Under these conditions, the series of nine divisions that form the endosporic gametophyte takes place synchronously within the spore population, with one division every 30 min. Samples were fixed at 5-min intervals after 4–4.75 h of growth in an attempt to find all stages of the last spermatogenous mitosis. Microspores were removed from growth solutions before fixation either by filtering them onto a 44-μm nylon mesh (Nitex, obtained from Tobler, Ernst & Traber, Inc., New York) mounted in a Millipore filtering apparatus (Millipore Corp., Bedford, Mass.) or by pelleting them by configuration.

Seeds of *Hordeum vulgare* cv. "Early Bonus" were germinated in petri dishes on filter paper moistened with distilled water. When coleoptiles were 10–18 mm long, usually after 2 d of growth at 20–25°C, the coleoptile and the enclosed primary leaf were excised 2 mm from the point of attachment to the seed. The area of the primary leaf epidermis undergoing stomatal complex-forming divisions is found within the next 2-3 mm from the cut edge. This segment of the leaf, still enclosed within the coleoptile, was cut into fixative and the coleoptile was slit open and discarded.

Fixation in Antimonate Solutions

Fixation and all subsequent aqueous steps were done in the presence of potassium antimonate according to Stoeckel et al. (47). Potassium antimonate was obtained from Fisher Scientific Co. (Pittsburgh, Pa.) (certified grade, pyro), lot 730312; Tridom (Fluka A.G., Basel, Switzerland; purissima, pyroantimonate); Polysciences, Inc. (Warrington, Pa.) (pyroantimonate), lot 157-9; and Pfaltz & Bauer Inc. (Stamford, Conn.). Simson and Spicer (43) report that sources of antimonate and even different batches from the same company are quite variable in their ionic strength and ability to precipitate cations. We have had successful precipitation with all four of these antimonate sources. Potassium antimonate was heated nearly to boiling in potassium phosphate buffer, pH 6.8, cooled, and added to glutaraldehyde to produce a fixative containing 5% glutaraldehyde, 2% antimonate and 0.1 M phosphate, pH 7.5–7.8. *Marsilea* microspores were fixed for 25 min on ice or at room temperature while *Hordeum* leaf segments were fixed for 2 h at room temperature.

Tissues were rinsed in 2.5% antimonate in 0.05 M phosphate buffer, pH 7.4–7.8. Antimonate was heated, as described above, to dissolve it. Postfixation was carried out for 1 h at room temperature in 1% OsO_4, 1.5% antimonate in 0.03 M phosphate buffer, pH 7.8. Final rinse and storage was done in 2.5% antimonate in 0.05 M phosphate buffer.

Dehydration and Embedment

Marsilea microspores were broken open in a French pressure cell (American Instrument Co., Silver Spring, Md.) operated at 3,000–5,000 lb/in^2 to allow subsequent infiltration of embedding medium into individual spermatogenous cells. Stoeckel et al. (47) reported that antimonate stain is readily lost from the edges of a tissue block; because *Marsilea* must be handled as single cells during dehydration and embedding, the danger of losing stain during processing is increased. To minimize loss, cells and microspore wall fragments were centrifuged at 5,000 g into a compact pellet for subsequent handling.

Dehydration was done quickly (5–10 min/step), using small volumes of fluid, according to the following scheme: three changes of 100% 2-methoxyethanol, one each of 100% 2-methoxyethanol:ethanol 1:1, 100% ethanol, and 100% ethanol:propylene oxide 1:1, and three of propylene oxide. Embedment was made in Epon-Araldite or Luft's Epon, using a flat-embedment protocol (15) in which the material is held in a thin layer of plastic between two glass slides that have been coated with MS 122 release agent (Miller-Stephenson Chemical Co. Inc., Danbury, Conn.). With *Marsilea* samples, areas for analysis were chosen from the center of the now-flattened pellet of cells. Silver sections were cut on a Reichert OM-U2 (Reichert Optical Works, Vienna, Austria) or a Sorvall "Porter-Blum" MT2-B ultramicrotome (DuPont Instruments-Sorvall, DuPont Co., Newtown, Conn.), counterstained with uranyl acetate and lead citrate, and examined with a Hitachi HU-11E, a Siemens 102, or a Philips 300 electron microscope operated at 75–80 kV.

Preparation of Standards, Chelator Treatment of Standards, and Tissues

Various cation-antimonate precipitate standards were made to allow comparison of their solubility properties with those of antimonate precipitates formed *in situ* in tissues. A 1-M solution of KCl, $CaCl_2$, or $MgSO_4$ was added to an equal volume of 2.5% potassium antimonate in 0.05 M potassium phosphate buffer, pH 8.0 (100 mM Sb, 175 mM K total). Under these conditions, pH remained in the 7.8–8.0 range during the precipitation reaction. The resultant antimonate precipitates were pelleted by a brief centrifugation. Standards were dehydrated and embedded in Epon-Araldite following the same procedures as used for tissue samples, and ultrathin sections were examined with a Zeiss EM-9A microscope.

The ability of divalent cation chelators to dissolve standards and intracellular deposits was investigated by floating grids on solutions of 0.2 M EDTA or 0.2 M EGTA, pH 7.9–8.0 at 60°C for 1 h. Distilled water, its pH adjusted to 8.0 with KOH and used under conditions identical to those of chelators, served as a control. After treatment, grids were rinsed briefly with distilled H_2O, and those containing tissue sections were counterstained as usual.

To allow a valid comparison of the appearance of cation-antimonate standards before and after various treatments, all prints were made on the same contrast grade of photographic paper, with the same enlarger aperture and development time. Print exposure times were adjusted so that the background Epon-Araldite had approximately the same density in all pictures: contrast between precipitates and background of each print was thus a reflection of the state of the precipitates themselves and not a function of the printing process. Likewise, any reduced contrast after chelator treatment reflected an actual change in the precipitates (i.e., some degree of dissolution by the chelator). Chelator-treated grids of *Hordeum* or *Marsilea* sections were also printed as above.

Assessment of Precipitate Distribution

In an attempt to quantify the degree of nonrandomness of antimonate localization, two approaches were employed. In the first, we counted the number of precipitates associated with organelles and the ground cytoplasm in a characteristic picture and calculated the percentage of total area occupied by the various compartments. This was done by tracing the nucleus, mitochondria, and blepharoplast, cutting them out, and weighing them and the remainder area of ground cytoplasm plus ER + nuclear envelope (NE). We estimated the area of ER + NE by determining their total length with a map tracer, multiplying this figure by the average width of an ER cisterna, and multiplying this product by 2 to include those areas of ER cut in grazing section. We then cut and weighed a rectangle of the same area as this. Subtracting this weight from that of the ER + NE plus cytoplasm provided an estimate of the area occupied by the cytoplasm.

The second approach involved placing a 2 × 5 cm mask over polar or intraspindle regions of a representative anaphase picture, and counting the total number of precipitates in each area.

RESULTS

Effects of Chelators on Cation Standards

Thin sections of embedded K^+, Mg^{++}-, and Ca^{++}-antimonate standards before and after treatment with water, 0.2 M EDTA, or 0.2 M EGTA at pH 8.0, 60°C, for 1 h are seen in Fig. 1.

While K^+-antimonate is normally quite soluble in warm water, embedded K^+-antimonate precipitates are not solubilized by distilled water (Fig. 1 b), EDTA (Fig. 1 c), or EGTA (Fig. 1 d); after any of these three treatments, samples look identical to untreated ones (Fig. 1 a).

After 1 h on distilled water (Fig. 1 f), Mg^{++}-antimonate
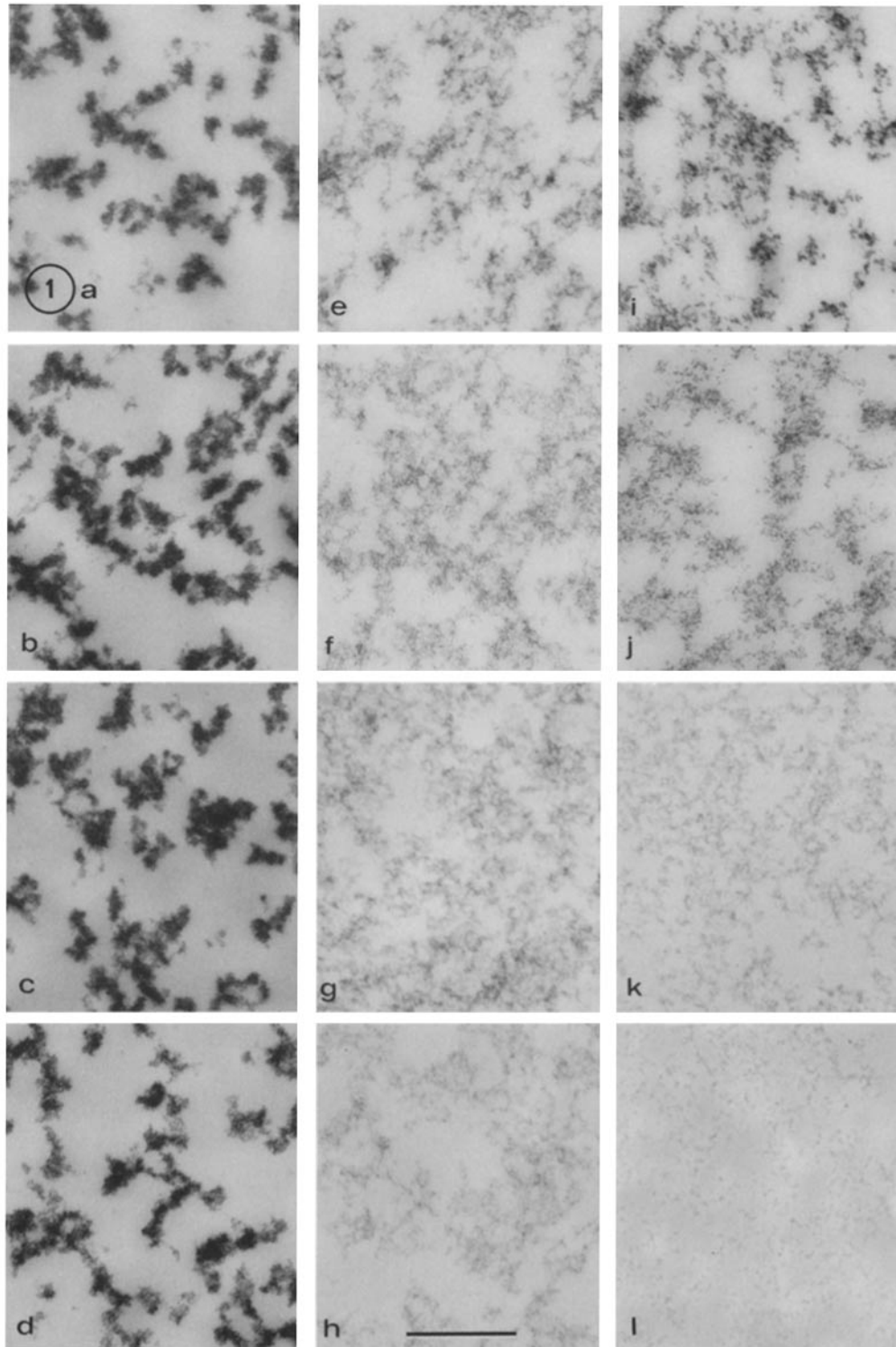
FIGURE 1   Appearance of thin sections of cation-antimonate standards before and after floating on distilled water, 0.2 M EDTA, or 0.2 M EGTA at pH 8.0, 60°C, for 1 h. (a) K^+-antimonate. (b) K^+-antimonate/water. (c) K^+-antimonate/EDTA. (d) K^+-antimonate/EGTA. (e) Mg^{++}-antimonate. (f) Mg^{++}-antimonate/water. (g) Mg^{++}-antimonate/EDTA. (h) Mg^{++}-antimonate/EGTA. (i) Ca^{++}-antimonate. (j) Ca^{++}-antimonate/water. (k) Ca^{++}-antimonate/EDTA. (l) Ca^{++}-antimonate/EDTA. × 32,400. Bars, 0.5 µm for Figs. 1, 2, and 5. Bars on all other Figs., 1 µm.

deposits look much like the original, untreated material (Fig. 1 e). EDTA (Fig. 1 g), likewise has very little effect on the appearance of Mg^{++}-antimonate, while EGTA partially dissolves the precipitates, as evidenced by the reduced electron density of precipitates against the background Epon-Araldite film in Fig. 1 h as compared to Fig. 1 e.

The effects of chelators on Ca^{++}-antimonate are more dramatic than their effects on Mg^{++}-antimonate. Distilled water treatment (Fig. 1 j) has little effect on the appearance of Ca^{++}-antimonate (Fig. 1 i), but EDTA (Fig. 1 k) produces a marked decrease in electron density, and EGTA (Fig. 1 l) nearly completely dissolves Ca^{++}-antimonate.

Effects of Chelators on Intracellular Deposits

When tissue sections are subjected to the same water and chelator treatments as the cation-antimonate standards, the intracellular antimonate precipitates are found to most closely resemble Ca^{++}-antimonate. Fig. 2 a is of a region adjoining a *Hordeum* anaphase chromosome, and displays antimonate deposits lining the ER elements among the kinetochore microtubules. After 1 h at 60°C in distilled water, pH 8.0 (Fig. 2 b), a section of a similar area shows no change in appearance of the precipitates, while EDTA (Fig. 2 c) and EGTA (Fig. 2 d) under the same conditions remove nearly all antimonate deposits. The only exception to this is found in cells known to accumulate nearly molar quantities of K^+, i.e., guard mother cells and guard cells of *Hordeum* (29, 32), in which a number of antimonate precipitates remain after treatment with either EGTA or EDTA.

Antimonate Localization through Mitosis in *Marsilea vestita*

We have chosen the last of the nine spermatogenous divisions of the *Marsilea vestita* microspore for this study. This particular division is marked by the presence of a blepharoplast at each spindle pole (15), and changes in these organelles as mitosis progresses aid in identifying the precise stage of mitosis, especially in spindles that have been sectioned obliquely. It also makes identification of polar areas possible in sections that, as a result of fixation at 4°C, do not contain microtubules. Another advantage of *Marsilea* as an experimental organism is the high degree of synchrony of mitosis among microspores in a population. This makes it possible to find several cells in the same stage of division in any given thin section.

Fig. 3 shows a cell in prophase of the ninth spermatogenous division. Nonrandomness of the antimonate reaction is easily visualized at this low magnification, with dense mitochondrial precipitates being most obvious. There are precipitates along the NE and scattered inside the nucleus and vacuoles, also. The large starch grains at the cell periphery do not react with antimonate. Extracellular materials at the cell surface stain densely, but in regions where the plasmalemma (PL) surface is free of extracellular materials, such as the lower left and upper right corners of Fig. 3, there are no antimonate deposits. At higher magnification, the association of antimonate with discrete membranous organelles is readily seen. While distinct membrane profiles are usually not found with the antimonate fixation as used here, there is a dilation of ER cisternae as well as of the space between inner and outer membranes of the NE and between inner and outer mitochondrial membranes. These dilated areas are less electron-dense than the surrounding

cytoplasm, nucleoplasm, or matrix. This makes it easy to see the ER and provides good contrast for the electron-opaque deposits of antimonate. During prophase, precipitates line the NE and elements of the ER adjoining the nucleus (Fig. 4). While the interior of each mitochondrion contains heavy deposits of antimonate, the outer membrane is in general devoid of precipitates, as is the ground cytoplasm. The blepharoplast, a microtubule-organizing center (MTOC) for the spindle of the ninth division (15), likewise does not contain precipitates (Fig. 4).

Nonrandomness of distribution of the antimonate reaction product was analyzed for Fig. 4. As can be seen in Table I, mitochondria contain 61% of the total number of antimonate deposits visible, but occupy only 8% of the total area of the picture. The next highest degree of sequestration is provided by the ER + NE which have 28% of the precipitates while occupying only 5% of the total area. In contrast, the nucleus, blepharoplast, and ground cytoplasm contain a very small percentage of the total Ca^{++}-antimonate (11% altogether) relative to the 87% total area that they cover. If we momentarily set aside the mitochondria, the intense staining of which dominates both the picture and the statistics, the contrast between the degree of Ca^{++} localization on ER + NE and that on nonmembranous cellular components becomes even more dramatic. These calculations reveal that 72% of the nonmitochondrial deposits are associated with ER + NE, which occupy only 5.5% of the nonmitochondrial area.

Dictyosomal cisternae do not dilate with these fixation procedures in the way that some of the other intermembranous spaces of the cell do. Since the membranes are not very heavily contrast-stained either, dictyosomes are difficult to identify in this material. Occasionally, they can be found at edges of cells and recognized by a closely packed line of precipitates along one of the sacs of the complex. In other sections, the swollen tips of sacs are most heavily stained with antimonate (Fig. 5).

Figs. 6 and 7 are of prometaphase. A slightly oblique section through the spindle emphasizes the ER between the blepharoplast at the pole and the chromosomes (Fig. 6). This ER is very dilated and contains some much larger antimonate precipitates in addition to those of more typical size. A few deposits are also seen along the chromosomes. A longitudinal section from a peripheral area of the spindle (Fig. 7) illustrates the manner in which the ER elements with their associated antimonate surround the chromosomes.

The cell seen in Fig. 8 is in metaphase, as can be determined by the beginning of blepharoplast breakdown (15). ER surrounding and within the spindle is stained with antimonate. The mitochondria, as well as some areas of the ER, contain relatively few but quite large precipitates, while other areas of ER have instead numerous small deposits. Clear microtubule (MT) images are very rarely seen. This is apparently due not only to fixation on ice, which would be expected to eliminate most MTs, but also to the presence of antimonate itself. A metaphase cell fixed in the presence of antimonate at 20°C contains microtubules which are preserved somewhat better (Fig. 9), but they are still not so clearly visible as those fixed conventionally. Little or no antimonate staining of the cell is found.

The reforming NE of the telophase daughter cells has numerous associated precipitates (Fig. 10). The blepharoplast at the edge of the figure has by now nearly completed its transformation into basal bodies.
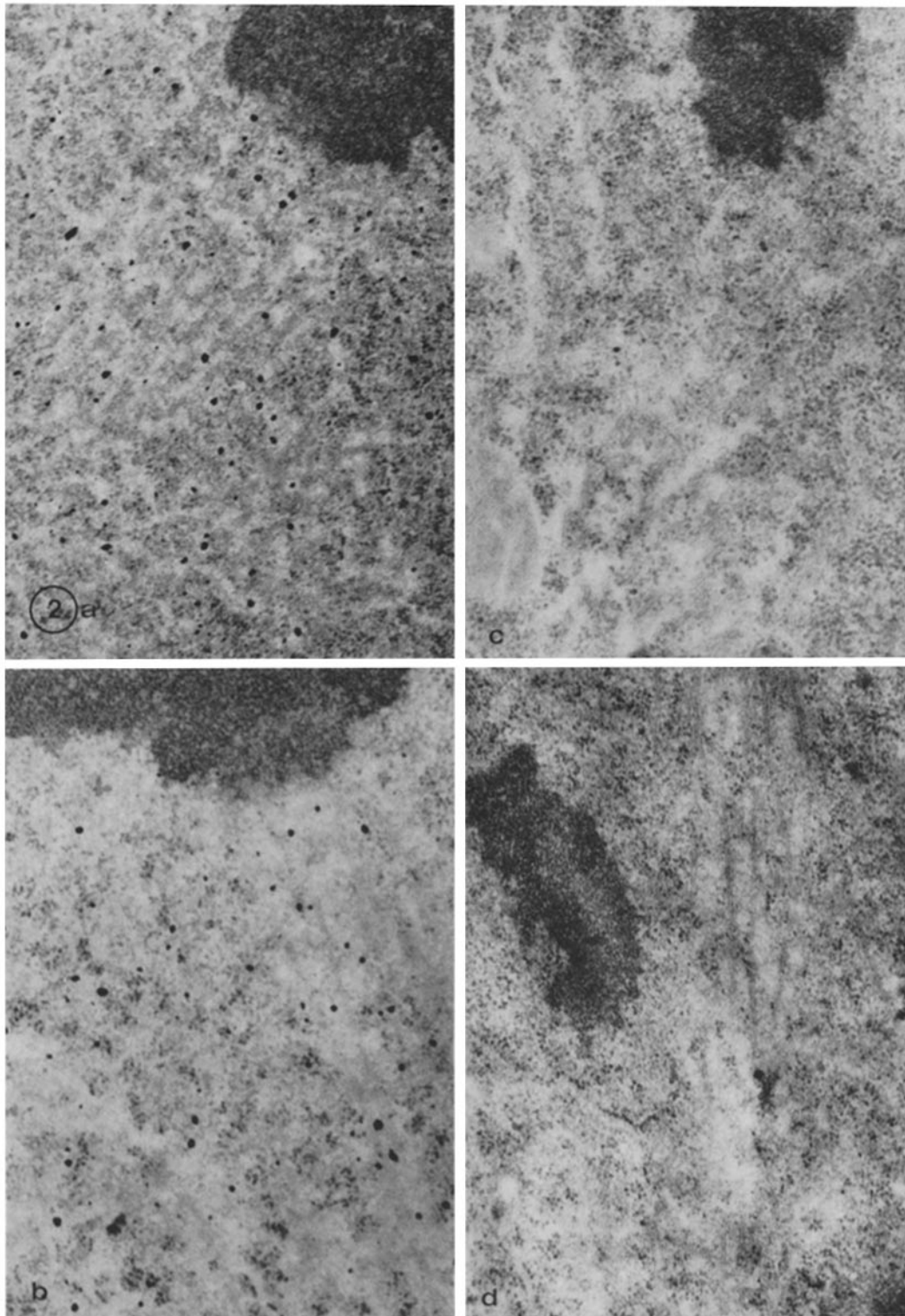
FIGURE 2 Appearance of intracellular antimonate deposits before and after treatment with distilled water, EDTA, or EGTA. Conditions are the same as those used for treatment of standards. All pictures are of *Hordeum* anaphase, and all include views of the ER that lies along kinetochore microtubules. (a) Untreated section, × 31,250. (b) Water treatment, × 29,200. (c) EDTA treatment, × 33,000. (d) EGTA treatment, × 30,000.

Antimonate Localization through Mitosis in Hordeum vulgare

One of the main positive attributes of the *Hordeum* stomatal complex system is the regularity of cell pattern within the complex and the predictability of the sequence and orientation of divisions along a segment of leaf blade. In a linear array of stomatal complexes, it is immediately possible to determine their relative ages because the ones positioned more distally along the leaf blade undergo division and differentiation before the more proximal complexes in the array (51, 52). This allows one to predict which divisions would have taken place next,
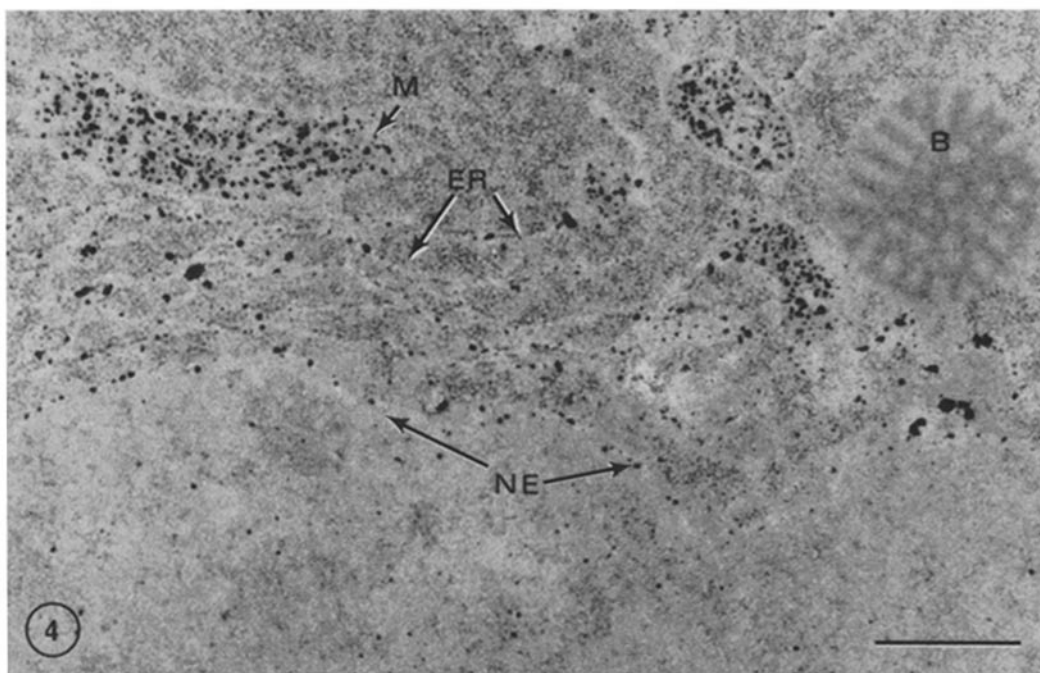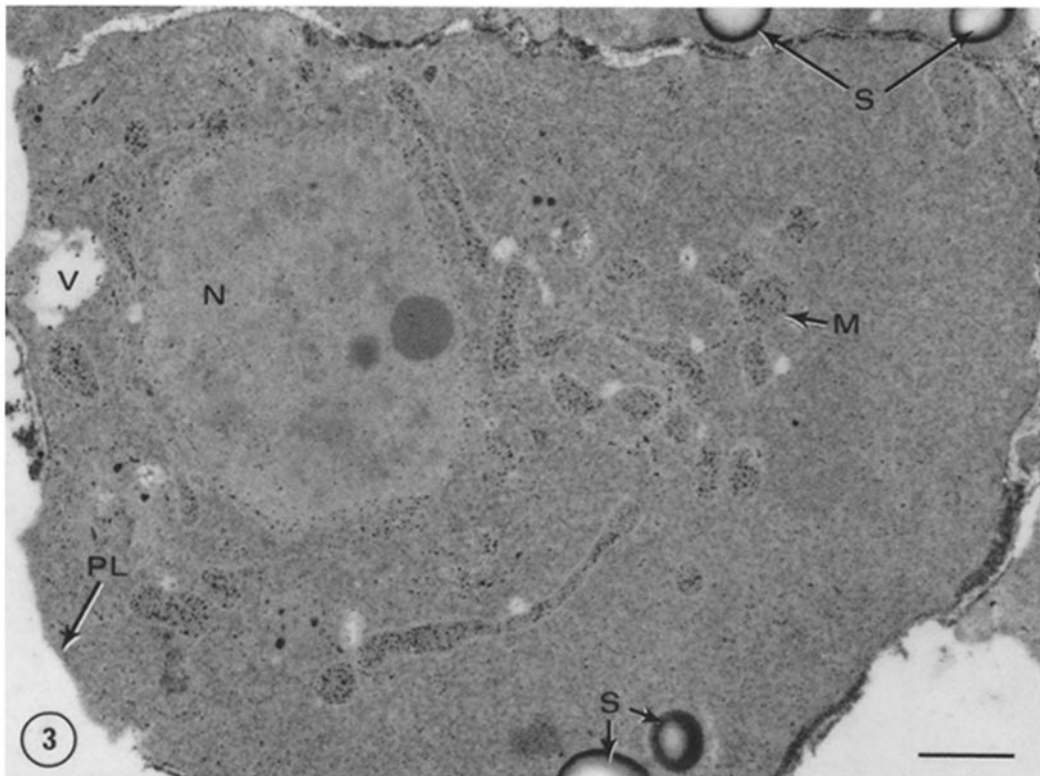
FIGURE 3   *Marsilea vestita* spermatogenous cell in prophase of ninth division. Mitochondria (*M*) have the most dense deposits of antimonate. Staining of NE, nucleus (*N*), and vacuoles (*V*) is also apparent. Starch grains (*S*) do not contain antimonate. PL itself is not stained, but intercellular material adjacent to it contains numerous deposits. × 13,000.

FIGURE 4   Higher magnification of prophase cell. Antimonate lines the NE and ER. Neither the blepharoplast (*B*) nor the outer mitochondrial membrane contain deposits. Note dilation of intermembrane spaces. × 39,500.

had the tissue not been fixed. The nucleus of the lateral cell must migrate into position alongside the guard mother cell (GMC) before it undergoes mitosis to give rise to a subsidiary cell of that GMC (51, 52). Because the spindle of the subsidiary cell division is always perpendicular to the file of cells containing the GMCs, we can determine not only where the nucleus

must end up before mitosis, but also the location of the poles before they are recognizable as such. This allows us to watch early stages in the development of the polar areas which in higher plants are unmarked by centrioles or any other discrete polar organelle.

The general pattern of antimonate precipitation in *Hordeum*

TABLE I

Distribution of Precipitates in Fig. 4

Subcellular compartment	No. of associated precipitates	Total area occupied by compartment	Total precipitates in compartment
		%	
Mitochondria	342	8	61
Nucleus	49	37	9
Blepharoplast	0	5	0
ER + NE	157	5	28
Ground cytoplasm	12	45	2
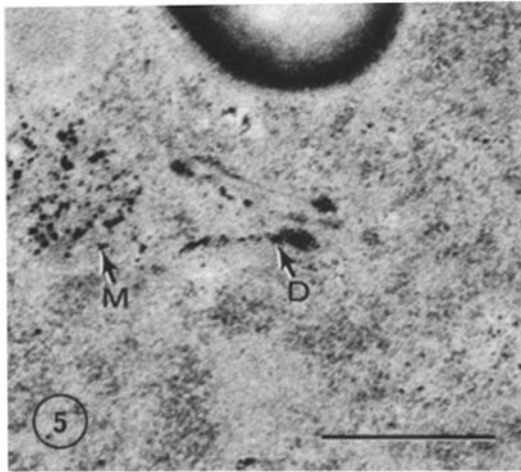
FIGURE 5   Dictyosomal profile. Antimonate deposits line one of the sacs of the dictyosome (D) and are also seen at the tips of sacs. M, mitochondrion. × 46,300.

can be seen in Fig. 11, which includes several epidermal cells. The GMCs are seen to contain significantly more precipitates than any of the other cell types, and many of these precipitates are randomly scattered in the cell. This situation is present in GMCs almost immediately after their formation, and the deposits become increasingly dense as the GMC grows and divides to give rise to the stomatal guard cells. Stomatal guard cells (29, 32) and their initials (29) are known to accumulate very high concentrations of K^+ (up to molar levels), and many of these GMC deposits may thus represent precipitation of K^+, either by itself or in conjunction with other cellular cations.

Localization of antimonate on/in certain subcellular structures is apparent in other epidermal cells, however. Two differences between *Hordeum* and *Marsilea* are the reduced number of NE-associated deposits in *Hordeum* and the less intense precipitation within its mitochondria. With the procedures used here, electron density of the mitochondria is almost identical to that of the ground cytoplasm, and this coupled with the low level of antimonate stain makes it very difficult to discern *Hordeum* mitochondria at low magnifications (Fig. 11). The slightly more electron-dense plastids are more visible. They contain fewer antimonate deposits than do the mitochondria. The vacuole, which is much larger in differentiated *Hordeum* epidermal cells than it is in the *Marsilea* spermatid, contains a large amount of precipitate. Areas of noncondensed chromatin also have antimonate associated with them, while condensed chromatin and the nucleolus do not.

As in *Marsilea*, the majority of cellular membranes in *Hor-*

deum are very indistinct after treatment with antimonate: the NE, ER, mitochondrial membranes, and chloroplast envelope are recognizable only as spaces which are more electron-transparent than their surrounds. Areas of cytoplasm that may appear at low magnifications to have a random scatter of antimonate are seen at higher magnification (Fig. 12) to consist of irregular networks of ER cisternae and mitochondria, both of which contain precipitates. The tonoplast is likewise not clearly defined. The only membrane exhibiting a clear electron-dense profile in *Hordeum* is the PL. Fine deposits can be found along some segments of PL as well as in the extracellular spaces between the PL and wall.

Of special interest within the stomatal complex are the lateral cell and its progeny. The lateral cell nucleus in Fig. 12 has migrated into its final position adjacent to the GMC and has entered prophase. Regions that will give rise to the spindle poles do not yet appear much different from the rest of the lateral cell cytoplasm, which has numerous antimonate-stained mitochondria and ER, as well as plastids.

By anaphase, there are large amounts of ER in the polar areas (Figs. 13–15). In a count of precipitates in a 2 × 5 cm area of each pole and of the center of the spindle of a typical anaphase picture, we found that the polar areas contain 41 and 49% of the total (55 and 65 deposits), while the area counted within the spindle yields only 10% of the total number of precipitates (14 deposits). Sometimes, antimonate precipitates within the spindle are approximately of the same diameter as the ER-derived elements with which they are associated, and therefore obscure them. The presence of lamellae of ER in this region of the *Hordeum* anaphase MA has been clearly shown, however, in conventionally fixed material (16) and in osmium-ferricyanide-stained tissues (17). ER along the sides of the spindle also has deposits associated with it (top of Fig. 13).

Anaphase polar areas are seen at higher magnification in Figs. 14 and 15. Staining patterns of *Hordeum* MTOCs and their immediate vicinity are similar to those seen in *Marsilea*: kinetochores do not have associated antimonate, whereas nearby ER membranes do. As in *Marsilea*, MT profiles in *Hordeum* are quite indistinct after fixation in the presence of antimonate. Here, antimonate precipitation of cations can take place at 20°C, and fixation is routinely done at that temperature. The scarcity of clearly visible MTs is apparently a function of the presence of antimonate in fixation and postfixation steps, because tissue that has been processed in solutions with pH and concentration of buffers and fixatives identical to those used here, but without antimonate, shows a more normal number of MTs. (Pictures not included.)

At telophase, the nuclear antimonate-staining pattern returns to that seen in interphase: the NE and condensed chromatin do not have precipitates, while noncondensed areas of the nucleus do (Fig. 16). The phragmoplast demonstrates various types and degrees of staining. That seen in Fig. 16 has very fine precipitates within the fusing vesicles of the phragmoplast, similar to those found associated with mature cell wall and the PL, in addition to more typical-size precipitates associated with vesicles and cisternae in the near vicinity of the phragmoplast.

DISCUSSION

Ca⁺⁺ Identification and Intracellular Localization

Our results show that antimonate precipitates are associated with the nuclear regions of cells of both *Marsilea* and *Hordeum*
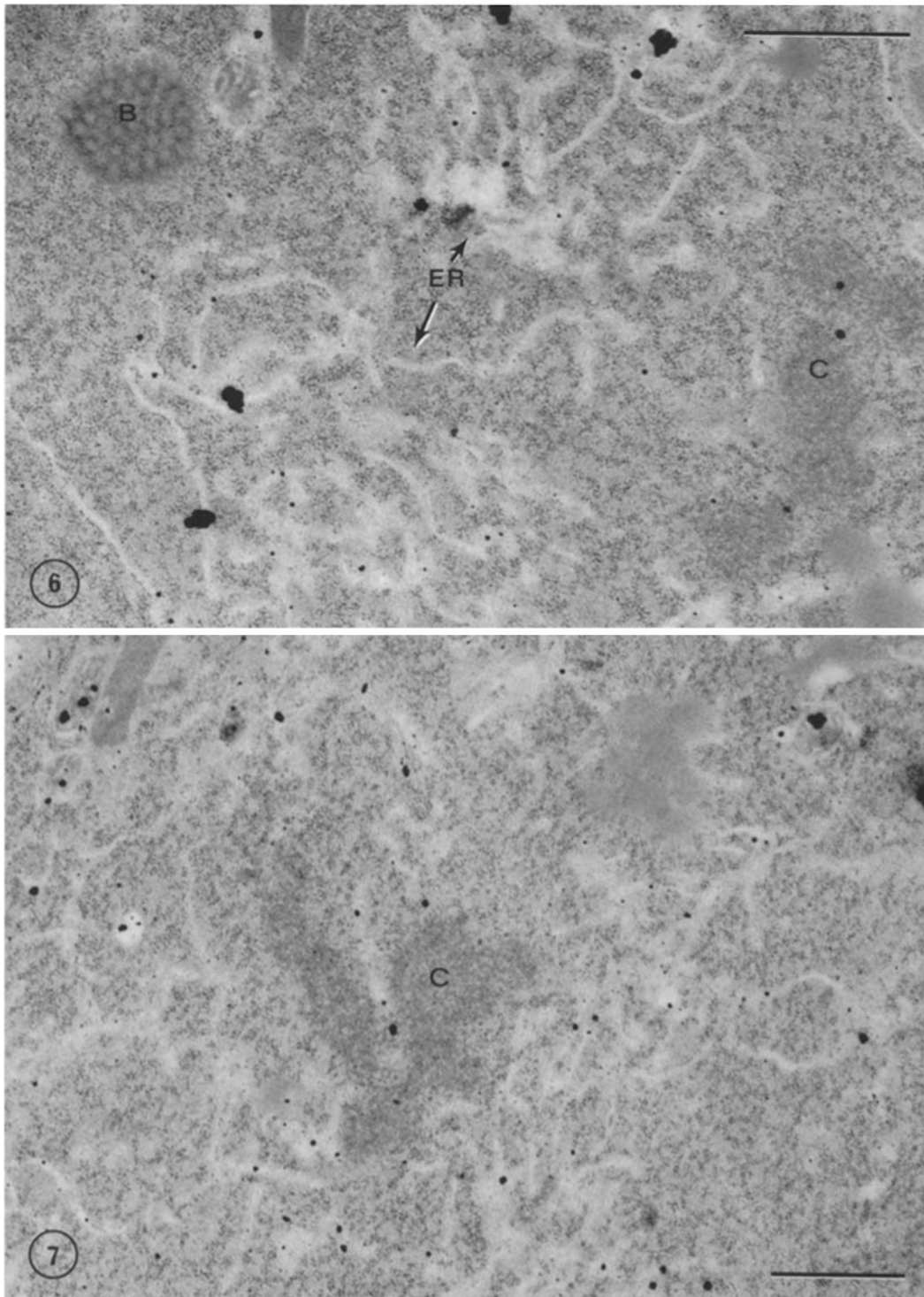
FIGURES 6 and 7 Prometaphase. In Fig. 6, dilated ER between chromosome (C) and blepharoplast (B) contains large and small deposits. Fig. 7 is the edge of the spindle. Close association of chromosomes and antimonate-containing ER is apparent. Fig. 6, × 25,100; Fig. 7, × 20,200.

throughout the cell cycle, as well as with mitochondria, dictyosomes, cell wall, phragmoplast, PL, and ER. Based on our studies using chelators, these deposits appear to be Ca^{++}-antimonate. Like the three types of antimonate standards, intracellular deposits appear essentially unaffected by distilled water. Both EDTA and EGTA, however, cause the disappearance of all deposits associated with the ER in the chromosome-to-pole area, and these same effects are found in other antimonate-

containing areas of mitotic cells of *Marsilea* and *Hordeum*. Several other groups have reported that intracellular antimonate deposits that have been shown by x-ray analysis to contain Ca^{++} are not visible after either EGTA or EDTA treatment (7, 18, 47, 48); Wooding and Morgan (49) found similar results with EDTA. Embedded K^+-antimonate is not solubilized by distilled water or by chelators, and in vitro Na^+-antimonate is likewise unaffected by EDTA or EGTA (37, 47). Were K^+ or
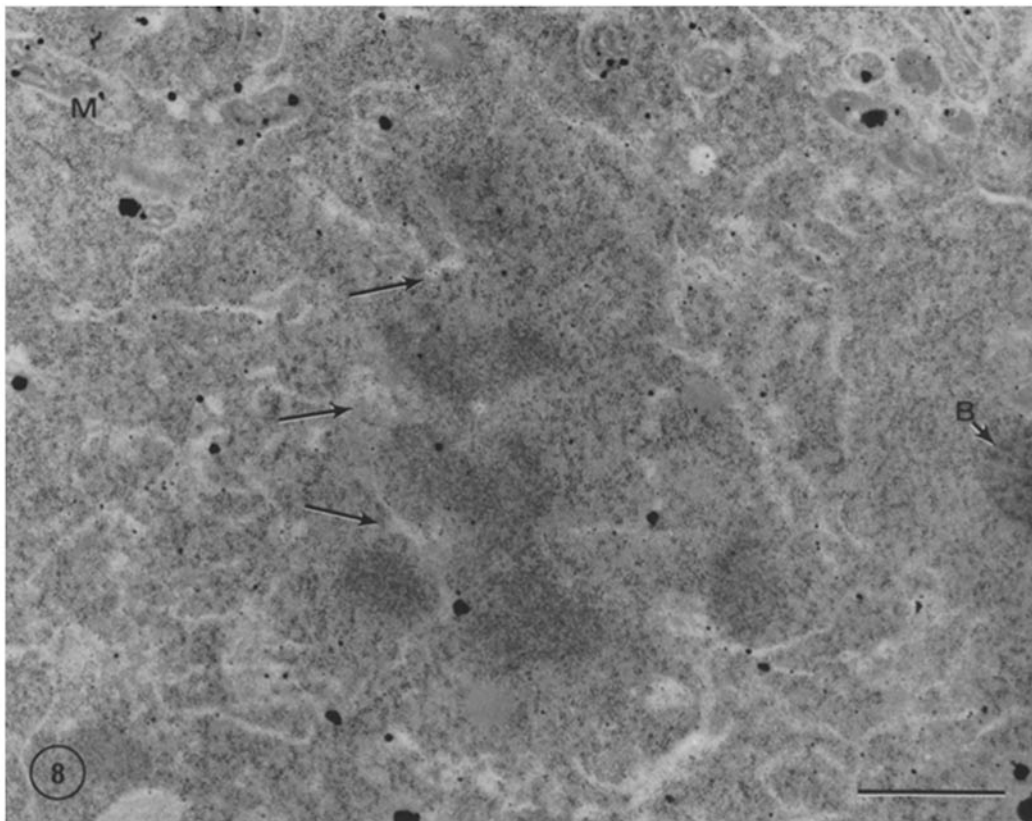
FIGURE 8 Metaphase. A blepharoplast (B) occupies the polar region and is beginning its transformation into basal bodies. ER with associated antimonate clearly surrounds the spindle. Elements of ER also extend among chromosome arms (arrows). Mitochondria (M) contain fewer deposits than seen earlier. × 19,600.
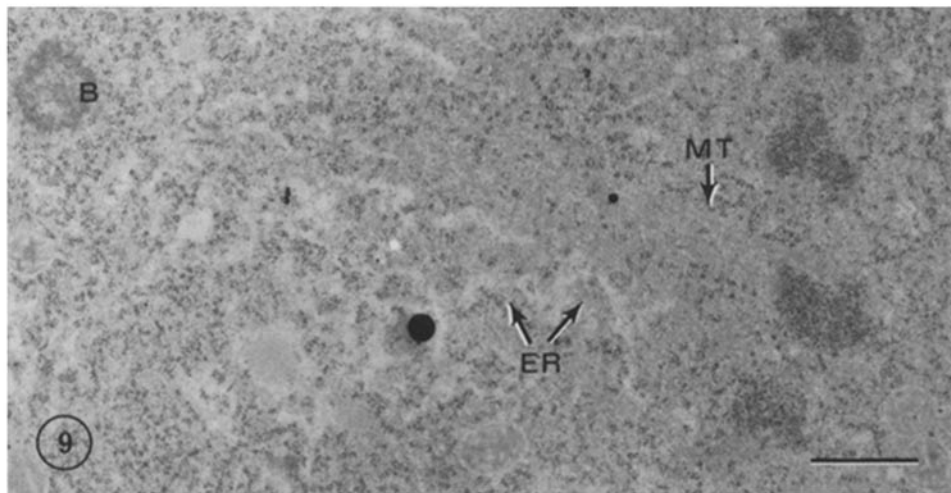
FIGURE 9 Metaphase of cell fixed according to antimonate procedure at 20°C. Essentially no antimonate precipitates are present. Close association between ER and MTs can be seen in central area of figure. B, transforming blepharoplast. × 14,700.

Na^+ contributing to formation of the intracellular antimonate precipitates we see, the deposits would remain after chelator treatment: this situation is seen only in *Hordeum* guard cells and GMC that are known to contain as much as 1 M K^+. We conclude that Ca^{++} is the major cation precipitated intracellularly by the specific variation of the antimonate technique used here.

While there is variation between *Marsilea* and *Hordeum* in the amount of antimonate associated with some types of organelles, the ER is similarly stained in the two species. The

close association of deposit-laden ER with the MA from beginning to end of mitosis is also readily apparent. Interphase and prophase precipitates on noncondensed chromatin and/or nucleoplasm and the NE are followed by an association of precipitates with the aggregates of reticular tubular elements of ER that occupy spindle pole areas as the NE breaks down. From prometaphase onward, the ER, which has been shown to invade the spindle interior and become closely associated with spindle MTS and chromosomes (12, 14, 16, 17, 50), likewise contains antimonate in both *Marsilea* and *Hordeum*.
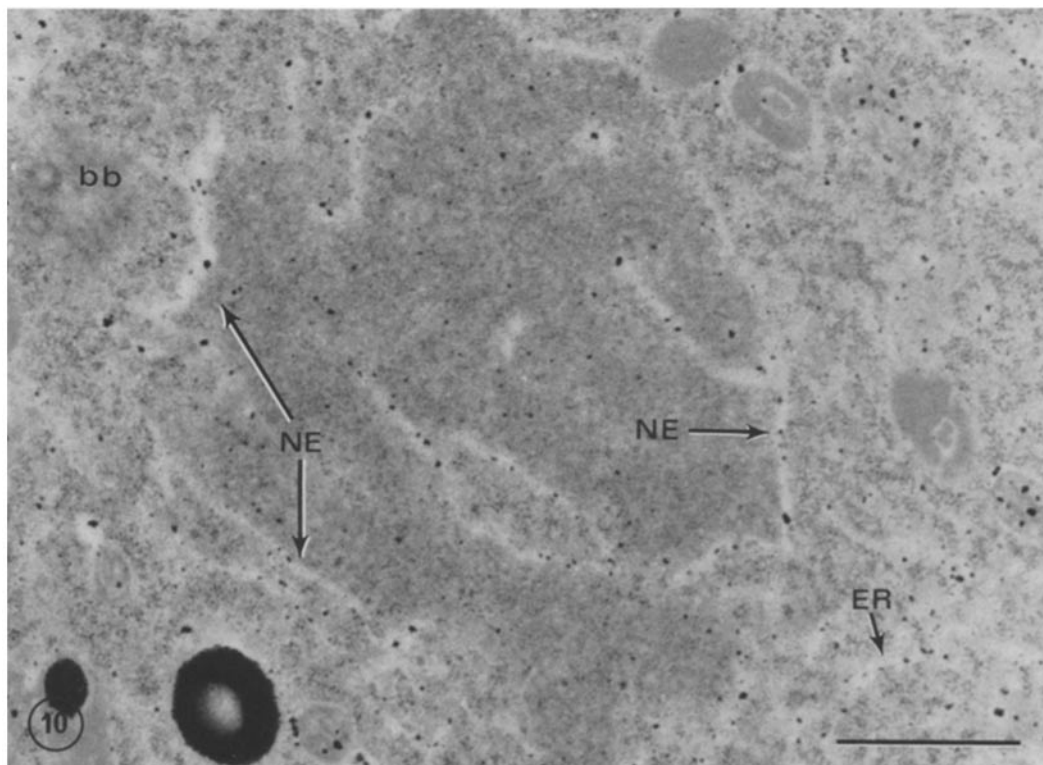
FIGURE 10   Telophase. Both the reforming NE and the surrounding ER contain many antimonate deposits. A few basal bodies (*bb*) from the nearly completely disintegrated blepharoplast are visible. × 24,800.

Precipitates are also found on the fragments of ER that lie directly alongside and partially envelop individual telophase chromosomes, and, when daughter nuclei form, there are again precipitates lining the *Marsilea* NE as well as being associated with the decondensing chromatin of both organisms. Other Ca^{++}-sequestering organelles, however, such as the mitochondria of *Marsilea*, are excluded from the region immediately surrounding the spindle throughout all stages of mitosis.

Because it is the organelle most similarly stained with antimonate between the two organisms, and because it is so intimately associated with the MA in both while other Ca^{++}-binding organelles are absent from the area, the ER appears to us to stand out from all the Ca^{++}-binding/sequestering membranous organelles as the one most possibly influential in the control of Ca^{++} levels in the MA.

Ca^{++} Buffering by ER

The suggestion that ER can in general function as a cellular Ca^{++}-buffering system is not without evidence. Any organelle proposed to take part in intracellular Ca^{++} regulation must have a high affinity for Ca^{++} binding and transport, and the ER has been shown to meet this requirement. The K_m for Ca^{++} uptake by ER has been found to be in the 0.3- to 5-μm range (2, 5, 9) and the ER ATPase can work *in situ* in very lightly fixed cells when Ca^{++} levels are as low as 1 μm (34). While the Ca^{++} affinities of ER and PL may be similar, the activity of the ER may predominate, especially in instances of rapid regulation, as its surface area is often several times greater than that of the PL (6, 9).

There is less detailed information concerning the Ca^{++}-buffering ability of ER at the specific time and in the specific locality of mitotic events. MAs from various cell types have been shown to contain a membrane-bound Ca^{++}-ATPase, the

activity of which cycles in accord with the cell cycle (25, 30). This raises the tantalizing possibility that membranous components of the MA are involved in Ca^{++} sequestration, and there is a recent report of such activity by vesicles of isolated MAs (41). The evidence for in vivo sequestration of injected Ca^{++} in spindle pole regions has been obtained using high (mM) Ca^{++} concentrations (20, 21), and whether this type of sequestration can occur at physiological Ca^{++} levels of μm or less likewise remains to be shown. Based on our results with antimonate showing that the ER in the MA, like the ER in the rest of the cell, does contain exchangeable Ca^{++}, and on the observation that the ER appears to be a structurally continuous system throughout the whole cell (17), it seems reasonable to conclude that spindle ER has a Ca^{++} affinity similar to that of bulk cellular ER, and that control of Ca^{++} levels within a physiological range by this spindle ER would be possible.

Ca^{++} Buffering by other Organelles

While the involvement of the ER with the MA makes it perhaps the most interesting subcellular compartment with respect to cellular Ca^{++} control, the involvement of other organelles in cell-wide regulation should not be dismissed. The suggestion that mitochondrial Ca^{++} uptake may not be the primary regulator of cellular Ca^{++} (2, 4, 9, 19, 26, 46) is particularly interesting in terms of plant cells, because Ca^{++} transport does not appear to be well-developed in most higher plant mitochondria (see reference 23 for review). The almost negligible amount of antimonate associated with *Hordeum* mitochondria lends support to this idea. In *Marsilea*, however, dense deposits associated with the mitochondria suggest that they have a high capacity for Ca^{++} sequestration and that, if Ca^{++} affinity is correspondingly high, they could play a major role in regulation of intracellular Ca^{++} fluctuations.
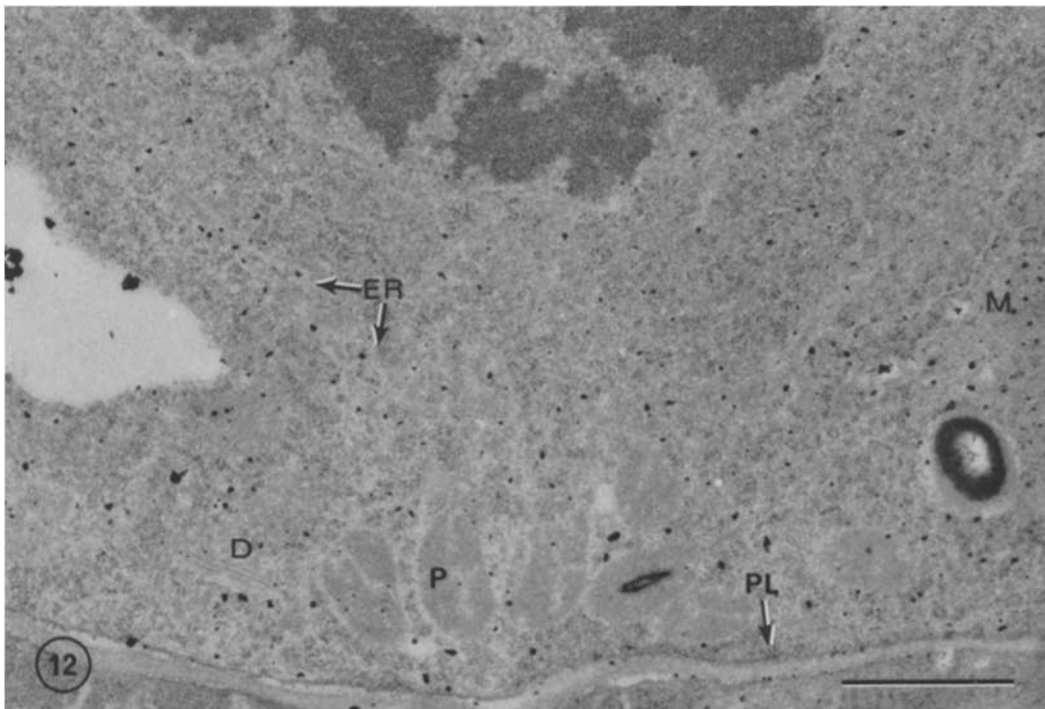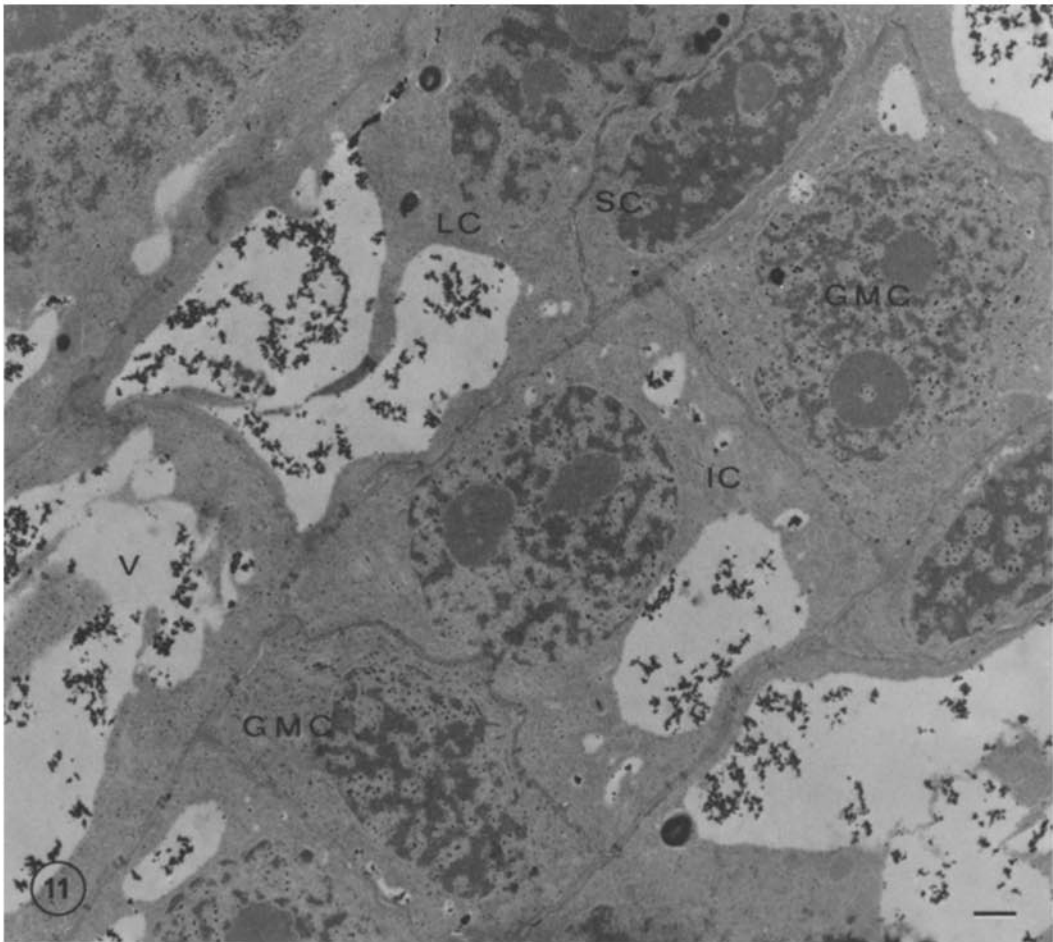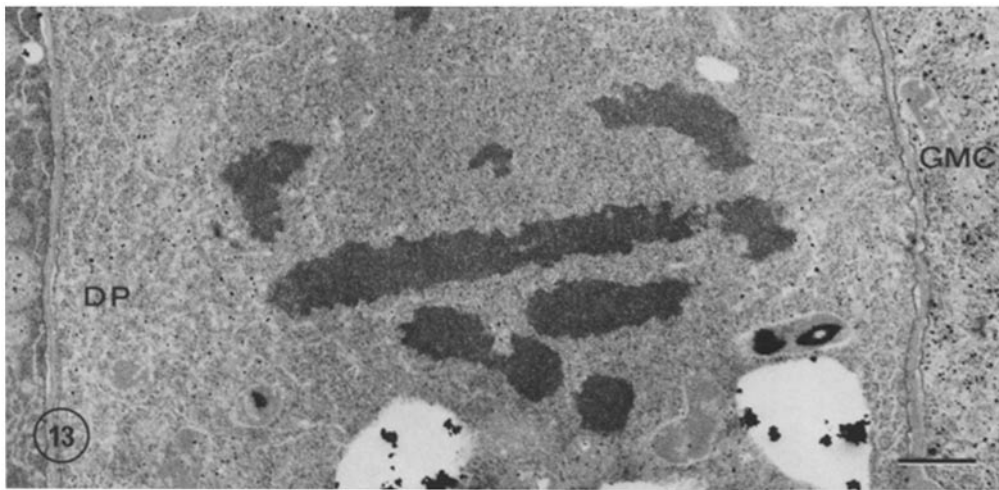
FIGURE 13 Whole anaphase spindle of a subsidiary cell division. Tremendous amounts of antimonate-containing ER occupy both polar areas, but especially the distal pole (DP). Precipitates in the intra-spindle region are also apparent. The GMC partially visible at the right contains a high density of random deposits. × 10,750.

FIGURE 14 The pole proximal to the GMC, same cell as in Fig. 13. Kinetochores (K) do not have associated deposits, while the ER immediately surrounding them does. The very fine precipitates of the PL and cell wall (CW) can also be resolved in this picture. × 22,000.
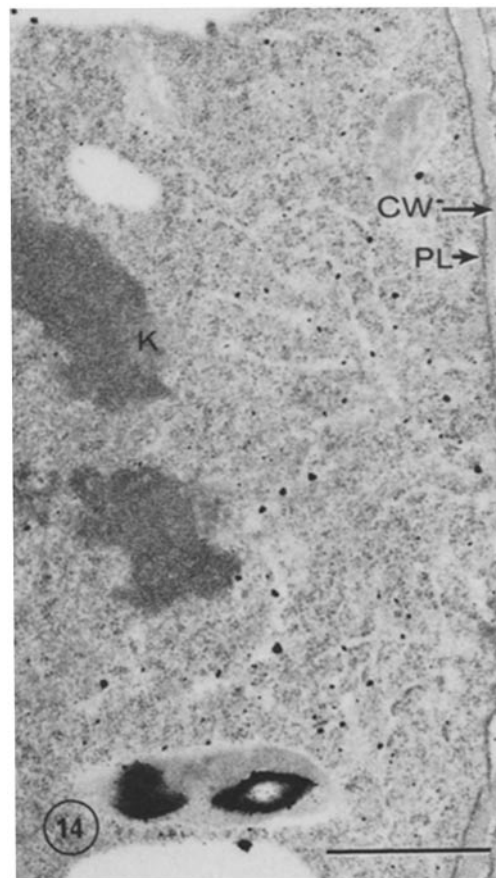
FIGURE 11 Low magnification view of Hordeum vulgare primary leaf epidermis. The three files of cells that give rise to stomatal complexes run obliquely across the figure. The central file is composed of alternating GMCs and intervening cells (IC). The file to either side of this one is made up of the much larger lateral cells (LC). The cell partially visible in the upper left corner is in an epidermal cell file which does not participate in stomatal complex formation. In the upper right corner is a GMC flanked by its two subsidiary cells (SC) which arise from division of the lateral cells. The next GMC down the file is younger, as evidenced by its size and shape as well as by its lack of subsidiary cells. The lateral cell nucleus that would have produced a subsidiary cell to the upper left of this GMC is at the opposite end of the lateral cell, out of the field of view. Vacuoles (V) contain the heaviest deposits of antimonate. At this magnification it is also possible to see precipitates in the euchromatin/nucleoplasm areas of the nucleus and the lack of deposits along the NE or on heterochromatin. Cytoplasmic antimonate appears to be denser in GMCs than in other cells. × 5,900.

FIGURE 12 Late prophase of a subsidiary cell-forming division. The interior of each mitochondrion (M) has antimonate associated with it, as do ER elements, seen as light channels against the ground cytoplasm. At this stage, the ER does not yet dominate the polar region; a dictyosome (D) and several plastids (P), containing little stain, are visible in the area which will become the distal pole. The PL is more electron-dense than any of the other cellular membranes, and precipitates can be seen between the PL and the cell wall. × 23,000.
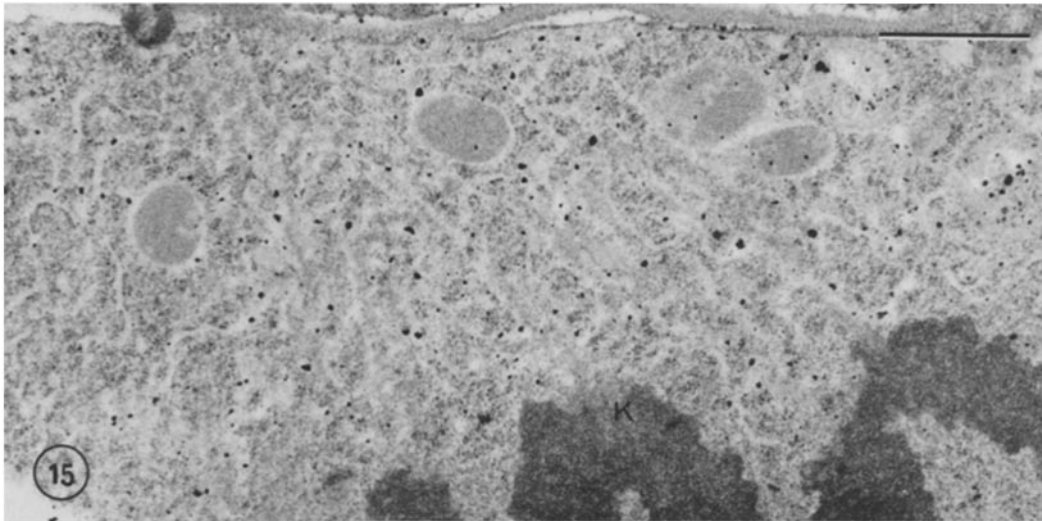
FIGURE 15 Distal pole of another subsidiary cell division. ER tubules and cisternae lined with precipitates lie immediately alongside MTs. The kinetochore (K) of the middle chromosome has been cut in grazing section. While there is antimonate on the ER adjacent to it, there is none associated with the kinetochore itself. × 20,500.
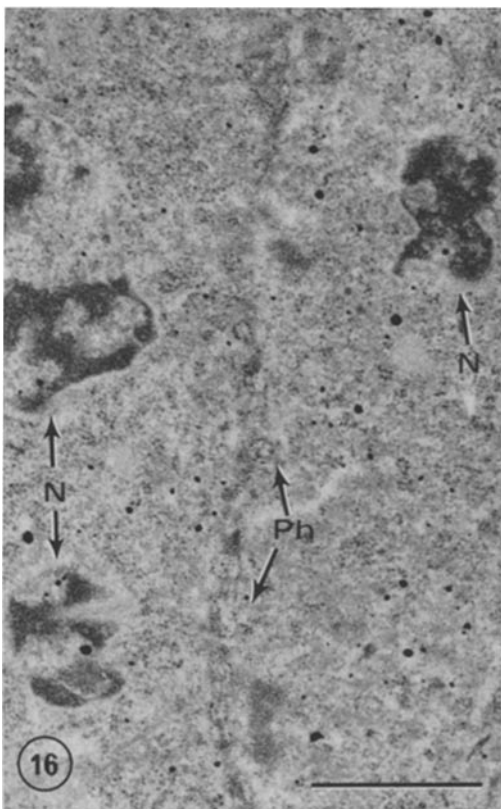

FIGURE 16 Telophase of subsidiary cell division. There is very fine staining of phragmoplast (Ph). Antimonate is also found on decondensing chromatin of reforming nuclei and in ER. Daughter nuclei (N) here are not yet spherical, and the section goes through more than one protuberance of the same nucleus. × 23,000.

An organelle in *Hordeum* which, with the ER, might be suspected of involvement in Ca^{++}-buffering activity on the basis of its staining with antimonate is the PL. The adjoining cell wall, with its relatively low affinity but very high capacity for Ca^{++} binding, could serve effectively as a sink for Ca^{++} extruded from the cell by action of PL transport systems. The

PL in this way would be suited for both long-term and high-capacity Ca^{++} buffering. It is also conceivable that Ca^{++} originally removed from cytoplasm and sequestered by the ER in a more central location in the cell could be shuttled to the PL and transported out to the wall, thereby increasing the long-range capacity of the ER's Ca^{++}-buffering activity. In terms of its distance from the spindle and its surface area which is smaller than that of the MA-associated ER, the PL with its adjacent wall is not likely to be the primary Ca^{++} regulatory system affecting mitosis, however.

While there is no typical plant cell wall separating spermatogenous cells of *Marsilea*, intercellular space within the microspore and the highly crenulate spore wall could likewise accommodate Ca^{++} transported out of cells. In instances in which several cells remain close to the wall after the spore has been ruptured to allow embedment, there are dense antimonate deposits seen in both areas.

Cellular structures that are interesting because of their lack of associated antimonate are kinetochores and the *Marsilea* blepharoplast. Any Ca^{++} control over the polymerization of MTs emanating from these MTOCs apparently is exerted by other elements, possibly by the ER found in close proximity to them, which shows evidence of Ca^{++} sequestration.

In summary, by means of antimonate precipitation, we have provided histochemical evidence for Ca^{++} binding or sequestration by various membranous organelles of dividing plant cells. As discussed further in a separate paper,[1] antimonate can be a very useful tool for the *in situ* localization of exchangeably bound Ca^{++}, i.e., the Ca^{++} that can be mobilized within the cell to effect regulation of Ca^{++}-sensitive processes. In view of the properties of precipitates formed under the procedures described here, we are confident that Ca^{++} is present in the antimonate reaction product visualized in our pictures. This study of *Marsilea* and *Hordeum* represents one of the few attempts at Ca^{++} localization in plant cells, and the first documentation of antimonate precipitation patterns throughout the stages of mitosis.

The similar antimonate staining of ER in both *Marsilea* and *Hordeum*, in spite of differences in other organelles with respect to their reaction with antimonate, suggests that ER may be commonly involved in intracellular Ca^{++} regulation. In partic-

ular, its intimate association with the spindle throughout all stages of mitosis and the exclusion of other Ca^{++}-binding/sequestering organelles from the immediate vicinity make the ER a prime candidate for Ca^{++} control within the MA. Furthermore, by virtue of the fact that antimonate-stained ER is found in so many regions of the MA (polar, peripheral, and internal), we conclude that this ER could bring about the effective regulation of Ca^{++} levels within microdomains of the spindle, such as in the immediate vicinity of MOTCs, which do not appear to bind exchangeable Ca^{++} themselves.

REFERENCES

1. Baker, P. F., and A. E. Warner. 1972. Intracellular calcium and cell cleavage in early embryos of *Xenopus laevis*. *J. Cell Biol.* 53:579–581.
2. Blaustein, M. P., R. W. Ratzlaff, and E. S. Schweitzer. 1978. Calcium buffering in presynaptic nerve terminals. II. Kinetic properties of the nonmitochondrial Ca sequestration mechanism. *J. Gen. Physiol.* 72:43–66.
3. Borle, A. B. 1973. Calcium metabolism at the cellular level. *Fed. Proc.* 32:1944–1950.
4. Brinley, F. J., Jr., T. Tiffert, and A. Scarpa. 1978. Mitochondria and other calcium buffers of squid axon studied *in situ. J. Gen. Physiol.* 72:101–127.
5. Bruns, D. E., J. M. McDonald, and L. Jarett. 1976. Energy-dependent calcium transport in endoplasmic reticulum of adipocytes. *J. Biol. Chem.* 251:7191–7197.
6. Carafoli, E., and M. Crompton. 1978. The regulation of intracellular calcium. *Curr. Top. Membr. Transp.* 10:151–216.
7. Cramer, E. B., and J. I. Gallin. 1979. Localization of submembranous cations to the leading end of human neutrophils during chemotaxis. *J. Cell Biol.* 82:369–379.
8. Doree, M., M. Moreau, and P. Guerrier. 1978. Hormonal control of meiosis. *In vitro* induced release of calcium ions from the plasma membrane in starfish oocytes. *Exp. Cell Res.* 115:251–260.
9. Farber, J. L., S. K. El-Mofty, F. A. X. Schanne, J. J. Aleo, Jr., and A. Serroni. 1977. Intracellular calcium homeostasis in galactosamine-intoxicated rat liver cells. *Arch. Biochem. Biophys.* 178:617–624.
10. Fulton, B. P., and D. G. Whittingham. 1978. Activation of mammalian oocytes by intracellular injection of calcium. *Nature (Lond.).* 273:149–151.
11. Fux, T. 1974. Chromosome elimination in *Heteropeza pygmaea.* II. Ultrastructure of the spindle apparatus. *Chromosoma (Berl.).* 49:99–112.
12. Harris, P. 1975. The role of membranes in the organization of the mitotic apparatus. *Exp. Cell Res.* 94:409–425.
13. Harris, P. 1978. Triggers, trigger waves, and mitosis: a new model. *In* Monographs on Cell Biology. Cell Cycle Regulation. J. R. Jeter, Jr., I. L. Cameron, G. M. Padilla, and A. M. Zimmerman, editors. Academic Press, Inc., New York. 75–104.
14. Harris, P., and D. Mazia. 1962. The finer structure of the mitotic apparatus. *In* Symposium on International Society of Cell Biology, Vol. 1. The Interpretation of Ultrastructure. R. J. C. Harris, editor. Academic Press, Inc., New York. 279–305.
15. Hepler, P. K. 1976. The blepharoplast of *Marsilea*: its *de novo* formation and spindle association. *J. Cell Sci.* 21:361–390.
16. Hepler, P. K. 1977. Membranes in the spindle apparatus: their possible role in the control of microtubule assembly. *In* Mechanism and Control of Cell Division. T. Rost and E. M. Gifford, Jr., editors. Dowden, Hutchinson and Ross, Inc., Stroudsburg, Pa. 212–232.
17. Hepler, P. K. 1980. Membranes in the mitotic apparatus of barley cells. *J. Cell Biol.* 86:490–499.
18. Hoffstein, S. T. 1979. Ultrastructural demonstration of calcium loss from local regions of the plasma membrane of surface-stimulated human granulocytes. *J. Immunol.* 123:1395–1402.
19. Janis, R. A., D. J. Crankshaw, and E. E. Daniel. 1977. Control of intracellular Ca^{++} activity in rat myometrium. *Am. J. Physiol.* 232:C50–58.
20. Kiehart, D. P., and S. Inoué. 1975. Microtubule depolymerization in local regions of the mitotic spindle by Ca^{++} microinjection. *Biol. Bull.* 149:433.
21. Kiehart, D. P., and S. Inoué. 1976. Local depolymerization of spindle microtubules by microinjection of calcium ions. *J. Cell Biol.* 70(2, Pt.2):230a (Abstr.).
22. Laetsch, W. M. 1967. Ferns. *In* Methods in Developmental Biology. F. H. Wilt and N. K. Wessells, editors. Thomas Y. Crowell, New York. 319–328.
23. Lehninger, A. L., B. Reynafarje, A. Vercesi, and W. P. Tew. 1978. Transport and accumulation of calcium in mitochondria. *Ann. N. Y. Acad. Sci.* 307:160–176.
24. Loewenstein, W. R., and B. Rose. 1978. Calcium in (junctional) intercellular communication and a thought on its behavior in intracellular communication. *Ann. N. Y. Acad. Sci.* 307:285–307.
25. Mazia, D., C. Petzelt, R. O. Williams, and I. Meza. 1972. A Ca^{2+}-activated ATPase in the mitotic apparatus of the sea urchin egg (isolated by a new method). *Exp. Cell Res.* 70:325–332.
26. Moore, L., D. F. Fitzpatrick, T. S. Chen, and E. J. Landon. 1974. Calcium pump activity of the renal plasma membrane and renal microsomes. *Biochim. Biophys. Acta.* 345:405–418.
27. Moore, L., and I. Pastan. 1978. Energy-dependent calcium uptake by fibroblast microsomes. *Ann. N. Y. Acad. Sci.* 307:177–194.
28. Moreau, M., P. Guerrier, M. Doree, and C. C. Ashley. 1978. Hormone-induced release of intracellular Ca^{++} triggers meiosis in starfish oocytes. *Nature (Lond.).* 272:251–253.
29. Palevitz, B. A., and P. K. Hepler. 1976. Cellulose microfibril orientation and cell shaping in developing guard cells of *Allium*: the role of microtubules and ion accumulation. *Planta (Berl.).* 132:71–93.
30. Petzelt, C., and D. Auel. 1977. Synthesis and activation of mitotic Ca^{2+}-adenosinetriphosphatase during the cell cycle of mouse mastocytoma cells. *Proc. Natl. Acad. Sci. U. S. A.* 74:1610–1613.
31. Pickett-Heaps, J. D. 1967. Ultrastructure and differentiation in *Chara* sp. II. Mitosis. *Aust. J. Biol. Sci.* 20:883–894.
32. Raschke, K., and M. P. Fellows. 1971. Stomatal movement in *Zea mays*: shuttle of potassium and chloride between guard cells and subsidiary cells. *Planta (Berl.).* 101:296–316.
33. Rebhun, L. 1976. Calcium, sulfhydryls and the mitotic apparatus. *Am. Zool.* 16:469–482.
34. Reinold, M., and W. Stockem. 1972. Darstellung eines ATP-sensitiven Membransystems mit Ca^{2+}-transportierender Funktion bei Amöben. *Cytobiologie.* 6:182–194.
35. Requena, J., R. Dipolo, F. J. Brinley, Jr., and L. J. Mullins. 1977. The control of ionized calcium in squid axons. *J. Gen. Physiol.* 70:329–353.
36. Rose, B., and W. R. Loewenstein. 1975. Calcium ion distribution in cytoplasm visualized by aequorin: diffusion in cytosol restricted by energized sequestering. *Science (Wash. D. C.).* 190:1204–1206.
37. Saetersdal, T. S., R. Myklebust, N.-P. Justesen, and W. Olsen. 1974. Ultrastructural localization of calcium in the pigeon papillary muscle as demonstrated by cytochemical studies and X-ray microanalysis. *Cell Tissue Res.* 155:57–74.
38. Salmon, E. D. and R. Jenkins. 1977. Isolated mitotic spindles are depolymerized by μM calcium and show evidence of dynein. *J. Cell Biol.* 75(2, Pt.2):295a (Abstr.).
39. Salmon, E. D., and R. R. Segall. 1979. μM Ca^{2+} induces microtubule depolymerization and spindle fiber shortening in isolated mitotic cytoskeletons. *J. Cell Biol.* 83(2, Pt.2):377a (Abstr.).
40. Schatten, H., and G. Schatten. 1977. The mitotic apparatus: high resolution scanning electron microscopy of the surface. *J. Cell Biol.* 75(2, Pt. 2):284a (Abstr.).
41. Silver, R. B., W. Z. Cande, J. K. Holtz, and R. D. Cole. 1978. The molecular composition of the mitotic apparatus from developing sea urchin embryos. I. Isolation, and initial characterization of protein composition, included vesicles, and calcium uptake. *J. Cell Biol.* 79(2, Pt.2):299a (Abstr.).
42. Silver, R. B., and R. D. Cole. 1979. On the role of membrane-bounded vesicles within the mitotic apparatus of sea urchins. Calcium sequestration and crossbridges to microtubules. *J. Cell Biol.* 83(2, Pt.2):373a (Abstr.).
43. Simson, J. A. V., and S. S. Spicer. 1975. Selective subcellular localization of cations with variants of the potassium (pyro)antimonate technique. *J. Histochem. Cytochem.* 23:575–598.
44. Siracusa, G., D. G. Whittingham, M. Codonesu, and M. DeFelici. 1978. Local anesthetics and phenothiazine tranquilizers induce parthenogenetic activation of the mouse oocyte. *Dev. Biol.* 65:531–535.
45. Sisken, J. E., and S. S. VedBrat. 1977. On the effects of variations in intracellular and extracellular calcium ions on mitosis and cytokinesis of HeLa cells. *J. Cell Biol.* 75(2, Pt.2):263a (Abstr.).
46. Somlyo, A. P., A. V. Somlyo, H. Shuman, B. Sloane, and A. Scarpa. 1978. Electron probe analysis of calcium compartments in cryo sections of smooth and striated muscles. *Ann. N. Y. Acad. Sci.* 307:523–544.
47. Stoeckel, M. E., C. Hindelang-Gertner, H.-D. Dellmann, A. Porte, and F. Stutinsky. 1975. Subcellular localization of calcium in the mouse hypophysis. *Cell Tissue Res.* 157:307–322.
48. Weakley, B. S. 1979. A variant of the pyroantimonate technique suitable for localization of calcium in ovarian tissue. *J. Histochem. Cytochem.* 27:1017–1028.
49. Wooding, F. B. P., and G. Morgan. 1978. Calcium localization in lactating rabbit mammary secretory cells. *J. Ultrastruct. Res.* 63:323–333.
50. Zatsepina, O. V., V. Y. Polyakov, and Y. S. Chentsov. 1977. Some structural aspects of the fate of the nuclear envelope during mitosis. *Cytobiologie.* 16:130–144.
51. Zeiger, E. 1971. Cell kinetics, development of stomata and some effects of colchicine in barley. *Planta (Berl.).* 99:89–111.
52. Zeiger, E. 1971. Organelle distribution and cell differentiation in the formation of stomatal complexes in barley. *Can. J. Bot.* 49:1623–1625.